



# APPARATUS AND DEMONSTRATION NOTES

The downloaded PDF for any Note in this section contains all the Notes in this section.

John Essick, *Editor*

*Department of Physics, Reed College, Portland, OR 97202*

Articles in this section deal with new ideas and techniques for instructional laboratory exercises, for demonstrations and for equipment that can be used in either. Although these facets of instruction also appear in regular articles, this section is for papers that primarily focus on equipment, materials and how they are used in instruction.

Manuscripts should be submitted using the web-based system that can be accessed via the *American Journal of Physics* home page, <http://web.mit.edu/rhprice/www>, and will be forwarded to the ADN editor for consideration.

## Demonstration of the lateral AC skin effect using a pickup coil

Anne E. Blackwell, Andrew P. Rotunno, and Seth Aubin<sup>a)</sup>

*Department of Physics, William & Mary, 300 Ukrop Way, Williamsburg, Virginia 23187-8795*

(Received 5 October 2019; accepted 30 April 2020)

We present a simple demonstration of the skin effect by observing the current distribution in a wide rectangular strip conductor driven at frequencies in the 0.25–5 kHz range. We measure the amplitude and phase of the current distribution as a function of the transverse position and find that they agree well with numerical simulations: The current hugs the edges of the strip conductor with a significant variation in phase across the width. The experimental setup is simple, uses standard undergraduate physics instructional laboratory equipment, and is easy to implement as a short in-class demonstration. Our study is motivated by modeling ac magnetic near fields in the vicinity of a rectangular trace on an atom chip. © 2020 American Association of Physics Teachers.

<https://doi.org/10.1119/10.0001272>

### I. INTRODUCTION

While direct current (dc) flows uniformly through a conductor, a time-varying or alternating current (ac) travels preferentially along the skin of a conductor. Interactions between the alternating current, the associated magnetic field, and the induced electric field create transverse spatial variations in both the current's amplitude and phase. This behavior defines the *skin effect*, which has been known since the late 19th century,<sup>1–10</sup> and the current distribution has been characterized for various wire profiles. However, with the exception of a cylindrical conductor of circular cross section (i.e., round wire), numerical approaches<sup>11–24</sup> and approximations<sup>25–32</sup> are required to determine the current distribution.

Primary interest in the skin effect concerns the increase in ac resistance due to the effective decrease in the wire cross-sectional area. For example, a 1 mm diameter copper wire with a 1 GHz ac increases its resistance per unit length to about 2.6  $\Omega$ /m, a factor of 120 compared to dc, while decreasing the self-inductance by a similar factor.<sup>33</sup> At high frequencies, braided and Litz wire can help mitigate the skin effect, and printed circuit board designs must account for this effect. To this end, much of the research on this topic predicts and measures bulk observables, such as ac resistance as a function of frequency<sup>12,16,24,34</sup> or wave penetration depth.<sup>35</sup>

In contrast, our interest in the skin effect concerns the associated ac magnetic field in the vicinity of a ribbon-like wire. In our research on ac Zeeman forces, we manipulate ultracold atoms with radio-frequency (rf) magnetic near-fields generated by currents in the microfabricated 100  $\mu$ m

wide traces of an atom chip.<sup>36,37</sup> While probing such  $\mu$ m-scale rf fields is challenging,<sup>38</sup> basic near-field predictions involving the skin effect can be tested experimentally with lower frequencies at the mm-scale.

In a ribbon-like conductor, with a rectangular cross section that is much wider than its thickness, the skin effect tends to concentrate the current along the two edges of the ribbon [see Fig. 1(a)] and is referred to as the *lateral skin effect*. Notably, the current density does not hug the edges of the ribbon as tightly as in a bulk conductor (the traditional skin depth) and does not vary appreciably over the thickness of the ribbon.

In this paper, we present a simple method for probing the current distribution and phase due to the skin effect in a ribbon-like conductor. An amplified pickup coil detects the current distribution in the conductor by measuring the amplitude and phase of the ac magnetic near-field just above the conductor. Our experimental scheme requires only standard lab equipment and is sufficiently simple for implementation as a classroom demonstration or as an undergraduate lab exercise. Also, we compare our measurements with predictions from several numerical models of varying complexities and dimensionalities. Figure 1 shows the current density and magnetic near-field predictions for four models, which largely agree with each other.

Our experimental method works best for ribbon-like conductors, which generate a one-dimensional spatial variation of the current density, so long as the skin depth is larger than the conductor thickness. Our ribbon conductor dimensions fall in this lateral skin effect regime for all the frequencies that we consider. Our method is reminiscent of the one

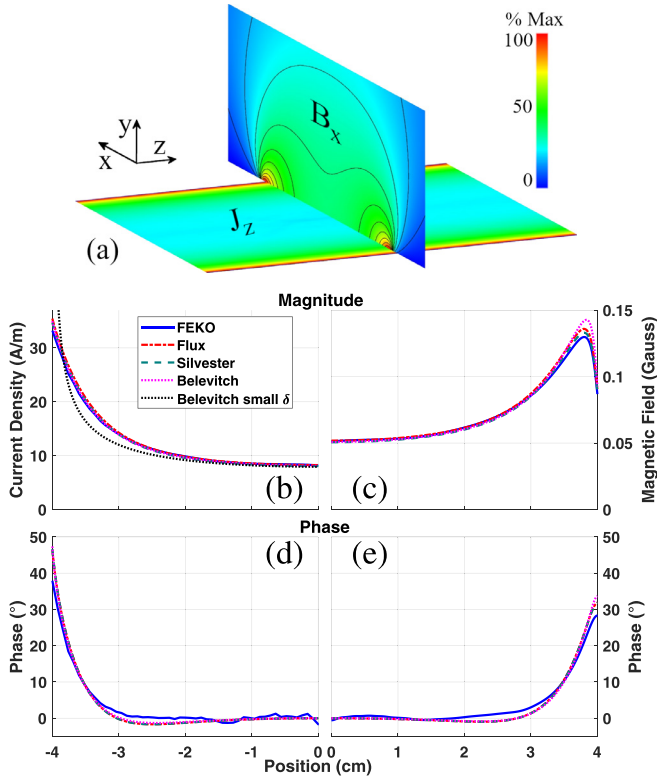


Fig. 1. Skin effect simulations for a 5 kHz ac of 1 A magnitude in our strip conductor (80.1 mm wide, 0.63 mm thick, and conductivity  $\sigma = 2.50 \times 10^7 (\Omega\text{m})^{-1}$ ). (a) False color maps of the current density  $J$  in the strip and magnetic field component  $B_x$  above it (FEKO simulation). (b) Plots of current density magnitude  $|J|$  vs position from edge to middle of the strip for four simulation methods (see Sec. II B). The black dotted curve is an analytic prediction in the 1D limit at high frequency. (c) Plots of magnetic field magnitude  $|B_x|$  vs position at a height of 0.8 mm. (d) and (e) Plots of relative phases vs position for  $J$  and  $B_x$ .

developed by Tsuboi and Kunisue<sup>39</sup> for analyzing magnetic fields produced by large ac in thin conducting plates.<sup>40</sup> Recent work has measured the skin effect in a stripline transmission line<sup>41</sup> and in a rectangular conductor at high current.<sup>42,43</sup> In contrast, Ampère's law and cylindrical symmetry guarantee that for a round wire, the external magnetic field is unaffected by the radial current distribution within it. In this case, direct measurements of the current density redistribution due to the skin effect must use an internal probe, such as neutrons,<sup>44</sup> NMR,<sup>45</sup> a liquid,<sup>46</sup> or a segmented<sup>35</sup> conductor, to name a few.

This paper is structured as follows: in Sec. II, we present the relevant electromagnetic theory and numerical approaches, followed by details of the experimental method in Sec. III. We present and compare our measurements of the current and magnetic field distributions with simulations in Sec. IV and conclude in Sec. V. The appendices provide additional details on the calibration procedure and also review analytic expressions for the skin effect and its phase distribution.

## II. THEORY

A straightforward classroom exercise is to take the curl of Faraday's law, combined with Ampère's law and Ohm's law, to arrive at

$$\nabla^2 \vec{J} = \sigma \mu \frac{d\vec{J}}{dt} = i\sigma\mu\omega \vec{J} = \frac{2i}{\delta^2} \vec{J}, \quad (1)$$

where  $\vec{J} = J(x, y)e^{i\omega t}\hat{z}$  is the longitudinally directed complex current density at angular frequency  $\omega$ , in a conductor of conductivity  $\sigma$  and magnetic permeability  $\mu$ . The equation can be written in terms of a single constant, the skin depth  $\delta = \sqrt{2/\sigma\mu\omega}$ , which sets a natural length scale for variations in current density. The diffusion relation in Eq. (1) gives two gifts: first, it directly shows that faster changes in the driven current create stronger spatial curvature of this current over distances of order  $\delta$ . Second, the sole dependence of Eq. (1) on the skin depth  $\delta$  gives rise to the principle of similitude,<sup>24,47</sup> which states that the current distribution in two different wires will be the same if they have the same dimensions in units of  $\delta$ . This allows for scaling of solutions to different sizes and frequencies. For example, an 8-cm wide pure aluminum strip [ $\sigma = 3.77 \times 10^7 (\Omega\text{m})^{-1}$ ]<sup>48</sup> with a thickness of 0.63 mm at 2.6 kHz ( $\delta = 1.6$  mm) will have the same current distribution when rescaled as a 40  $\mu\text{m}$  wide copper trace with a thickness of 0.32  $\mu\text{m}$  at 6.8 GHz ( $\delta = 0.8$   $\mu\text{m}$ ).

The round wire admits the only known exact analytic solution to Eq. (1) in a finite volume.<sup>29,49</sup> The round wire solution for the current density is given by  $J(r) = C\mathcal{J}_0[(1-i)r/\delta]$ , valid at all frequencies, where  $r$  is the radial coordinate,  $\mathcal{J}_0(r)$  is the Bessel function of the first kind, and  $C$  is a normalization constant. In the high frequency limit ( $\delta \ll R$ , for radius  $R$ ), this solution reduces to  $J(r) \simeq J_{\text{max}}e^{-(1+i)(R-r/\delta)}$  for  $r \simeq R$ , with  $J_{\text{max}}$  the current density at the edge of wire. Notably, this example shows that the phase of the current distribution also varies with  $r$  across the conductor, a fact that is often overlooked in discussions of the skin effect. Specifically, the phase wraps by  $2\pi$  for every  $\delta$  of penetration into the wire as its amplitude decreases by  $1/e$ . N.B.: at a given time, the current flow is not all in the same direction.

A ribbon-like conductor, with thickness  $2T$  much smaller than the width  $2W$ , is in the *lateral skin effect* regime for  $\delta \gg T$ .<sup>26</sup> In this case, the current distribution falls off from the two ribbon edges to a finite value in the middle with a  $1/e$  characteristic decay length  $\lambda$  that is larger than the skin depth  $\delta$ . While the fall off does not have a closed form, at low frequency ( $\delta^2 > WT$ ), it is roughly polynomial, while at high frequency ( $\delta^2 < WT$ ), it is more exponential-like. In the very high frequency limit ( $\delta^2 \ll WT$ ), the lateral current distribution has an analytic form (see Appendix A), which is plotted in black in Fig. 1(b). Notably, the phase also varies across the conductor width but less so than in the round wire case (see Appendix B and Fig. 9).

We have provided a supplemental online animation,<sup>50</sup> which illustrates the time-evolving nature of the current density's phase and amplitude across a wide range of frequencies. The lateral current density is shown to advance by rotating around the position axis in complex space [as in Fig. 2(e)]. The instantaneous amplitude is projected onto the real axis to show the measured value. Generally, the phase (and current) at the edges leads the current at the center of the strip. At very high frequencies, the total current lags 90° behind the near-dc phase (and current).

## A. Pedagogical explanation

We present a pedagogical explanation for the ac skin effect in Fig. 2 by expanding on an approach given by Zangwill.<sup>51</sup> The reason that an ac hugs the skin of a

conductor is because the driving current creates a magnetic field that is the largest at the edge, which, in turn, generates opposing eddy currents. The net result is a current distribution that is the largest in amplitude at the skin and out of phase with the source. To demonstrate further, we begin by considering a round wire (radius  $R$ ) driven by a low enough frequency  $\omega$  such that the skin effect is a small perturbation on the uniform current distribution (i.e.,  $\delta \gg R$ ). We can use the following steps illustrated in the indicated parts of Fig. 2 to calculate the first order correction to a uniform input current distribution  $J$  with a low frequency  $\omega$ :

- shows the sinusoidal time dependence of the uniform input ac, its associated magnetic field  $B$ , the first order contribution to the induced electric field  $\vec{\nabla} \times \vec{E}_{ind} = -d\vec{B}/dt$ , and the resulting eddy current  $\Delta J = \sigma E_{ind}$ .
- shows the uniform input ac density  $J = J_0 \sin(\omega t)$  and its in-phase quasi-static magnetic field  $B = B_0 \sin(\omega t)$ . The field  $B_0 = \mu J_0 r/2$  increases linearly outwards from the center.
- shows the spatial dependence of  $-dB/dt = -\omega B_0 \cos(\omega t)$ , which then generates an induced electric field  $E_{ind}$  (first order) via Faraday's law.
- shows the eddy current distribution  $\Delta J$  generated by  $E_{ind} = \mu J_0 \omega (r^2/4) \cos(\omega t)$  along the wire axis. Applying Ohm's law, we obtain the first order correction to the current density  $\Delta J = (J_0/2)(r/\delta)^2 \cos(\omega t)$ , which increases quadratically from the wire center.
- shows the resulting total current density  $J_{tot}$  from the quadrature sum of the input current  $J$  and the first order correction  $\Delta J$ .

Thus, to first order, the ac skin effect results in a current density  $J_{tot}$  that varies radially in *magnitude* as  $1 + (r/\delta)^4/8$  and radially in *phase* as well. As the drive frequency  $\omega$  is increased, higher order contributions in  $(r/\delta)^2$  must be included. The physics is similar for a strip conductor; however, the computation of  $J_{tot}$  is more involved.

## B. Simulations

Numerical approaches are required for calculations of  $J_{tot} = J(x, y)$  with an arbitrary conductor profile and often begin by converting Eq. (1) into an integral equation,<sup>15</sup>

$$J(x, y) = J_{dc} - \frac{i}{\pi \delta^2} \iint_A J(\tilde{x}, \tilde{y}) \ln \sqrt{(x - \tilde{x})^2 + (y - \tilde{y})^2} d\tilde{x} d\tilde{y}, \quad (2)$$

where the  $J_{dc}$  term is the uniform current density expected for a dc. The second term generates the skin effect by which the strip's self-inductance redistributes the current in the wire.

We compute  $J(x)$  using four different methods and then calculate the corresponding  $x$ -component of the magnetic near-field  $B_x(x, y_h)$ , evaluated at the effective height  $y_h$  of our pickup coil. Models that consider the vertical extent of  $J$  show less than a part in  $10^3$  variation vertically for our parameters, and this extent is averaged over for  $J(x)$  values.

We use two commercial electromagnetic solvers to compute  $J(x)$  and  $B(x, y_h)$ . FEKO uses a method of moments (MoM) approach to solve a finite-length model of our strip, giving the only longitudinal current description, but the

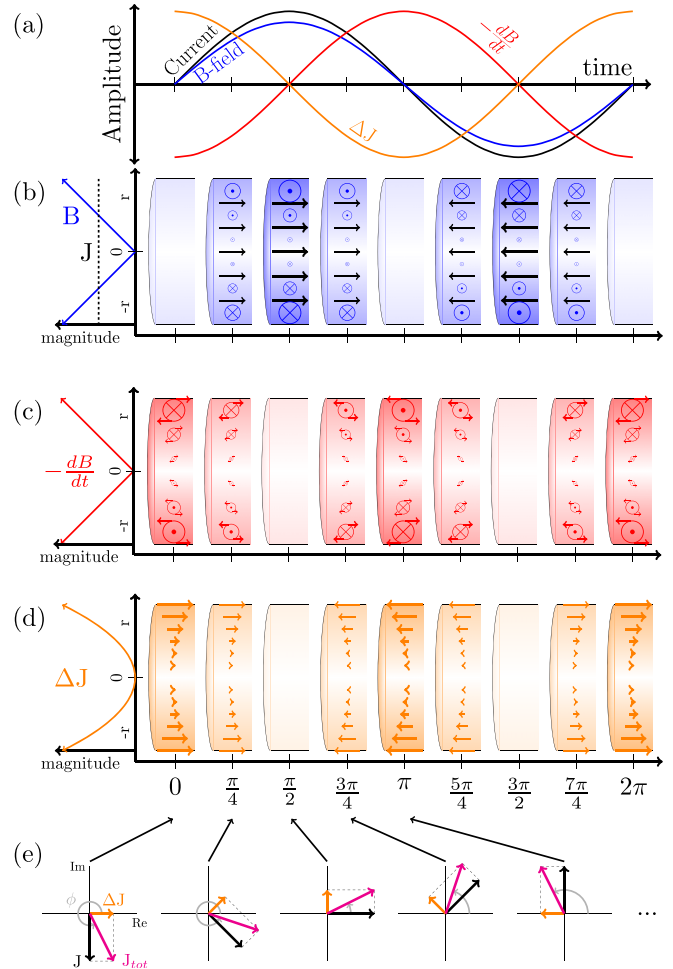


Fig. 2. Visual explanation of the ac skin effect at low frequency in a round wire. (a) Plot vs time of the input current, associated quasi-static magnetic field  $B$ , and the first order contributions to the induced EMF and eddy current  $\Delta J$ . (b) Quasi-static magnetic field  $B$  (blue) due to a uniform ac input current density  $J$  (black arrows) vs oscillation phase. (c) First order  $-dB/dt$  contribution (red) to the induced EMF from (b) vs phase. (d) Induced eddy current density  $\Delta J$  (orange arrows) from EMF in (c). (e) Complex-plane representation of the uniform input current density  $J$ , the first order eddy current density  $\Delta J$  contribution from (d) at fixed  $x$ , and resulting total current density  $J_{tot}$  (magenta) at various phases.

current sheet model gives no vertical information. FLUX uses a finite element method (FEM) to solve a 2D transverse cross section of the strip, without longitudinal information.<sup>52</sup>

We have also directly implemented two numerical algorithms that model an infinite length strip in the transverse plane. The first algorithm is by Silvester<sup>15</sup> and solves Eq. (2) by decomposing the strip cross section onto a Cartesian grid of square  $dx dy$  elements and calculating the mutual induction between them. The second algorithm by Belevitch *et al.*<sup>27</sup> uses a flat line of current expanded in even polynomial powers to solve the same equation (see Appendix A for a summary of this method).

We find that the four numerical models give comparable results for the phase and amplitude of the current density  $J(x)$  and magnetic field  $B(x)$  (see Fig. 1). Three of the models give very similar results, but we find that the FEKO phase results deviate somewhat from the others and depend on the discretization mesh geometry.<sup>53</sup> We note that the phase offsets of each model in Figs. 1(d) and 1(e) have been adjusted so that the phase over the center portion of the strip

corresponds to  $0^\circ$ . In the case of FEKO, the small contribution to the ac magnetic field from the supply wires is subtracted out in Figs. 1(c) and 1(e).

### III. EXPERIMENTAL METHOD

We measure the ac distribution  $J(x)$  (in A/m) laterally across a thin aluminum strip via the ac magnetic near-field that it produces at the surface of the conductor. We use a lab-built pickup coil located just above the strip to sample the ac magnetic field via the voltage induced in the coil.

The basic experimental setup [see Figs. 3(a) and 3(d)] consists of a thin strip of aluminum driven by a sinusoidal current source. The pickup coil is scanned transversely across the surface of the conducting strip, and its induced emf signal is sent to a battery-powered amplifier (gain  $\sim 10^4$  with 10 kHz bandwidth, based on two OP27E op-amp gain stages). The output of the amplifier is then displayed on an oscilloscope, along with the signal from an isolated Hall sensor (LEM model HX 10-NP) that monitors the total current through the strip. A series ammeter provides an additional rms measurement of the ac.

The aluminum alloy strip has width  $2W = 80.1(1)$  mm and thickness  $2T = 0.63(1)$  mm. We measure its dc conductivity to be  $\sigma = 2.50(6) \times 10^7 (\Omega\text{m})^{-1}$  with a four-point measurement. The aluminum strip is mounted on medium density fiberboard (MDF) with double-sided tape, and electrical connections soldered on washers are bolted to the strip

with through holes at its two ends. The strip is about 0.9 m long but could be much shorter since the pickup coil measures very little variation in the signal along the strip's length, except at the ends.

We direct an ac with an amplitude of 1.85 A ( $1.3 A_{rms}$ ) through the strip using a voltage controlled current source driven by the sinewave output of a function generator. At near-dc frequencies, the current density is essentially uniform at  $J_{dc} = 1.85 \text{ A}/8 \text{ cm} \approx 23.1 \text{ A/m}$ , which corresponds to a surface magnetic field of  $B_{dc} \approx 0.145 \text{ G}$ . We use drive frequencies in the range of 0.25–5 kHz. Our current source (lab-built, based on a LM675 op-amp) operates up to 5 kHz, while below 250 Hz, the small pickup coil signal is too noisy.

The amplified pickup coil is very sensitive to environmental noise, such as rf communication signals (e.g., Bluetooth and WiFi) and the 60 Hz noise (and associated harmonics) emanating from nearby electrical devices. We found that for low noise measurements, the overhead fluorescent lights and cellphones had to be turned off while taking data. Alternatively, in a noisy environment, directing the battery-powered amplifier signal to a lock-in amplifier could provide a cleaner signal.

Care was taken to route the ac supply wires away from the pickup coil to minimize crosstalk. We suspect that the placement of these supply wires on one side of the conductor may contribute to the slight asymmetry in the current distribution observed in Fig. 5.

#### A. Pickup coil

The pickup coil [Figs. 3(b) and 3(c)] consists of a machined, highly elongated rectangular copper loop of external dimensions of  $114 \text{ mm} \times 1.85 \text{ mm}$  with an inner gap measuring  $110.6(1) \text{ mm} \times 0.38(5) \text{ mm}$ , centered at a height of  $0.80(5) \text{ mm}$ . The base for construction was a  $114 \text{ mm} \times 79 \text{ mm}$  double-sided copper-clad electronics prototyping circuit board (PCB). We initially used two loops on the front and back in series for higher sensitivity but switched to a single loop for improved spatial resolution. The PCB construction ensures that the pickup loop is flat in a plane and that the two coil planes are parallel.

We machined the PCB into the pickup coil using a desktop CNC milling machine (Carvey, Inventable Inc.). Bulk copper removal was done with a regular end mill bit ( $1/8''$  fishtail upcut bit), while a specialized 0.1 mm diameter bit (P3.2501) was used for the regions directly adjacent to the wire loop and within it.

We note that alternative single-turn and multi-turn pickup coils based on wrapping a thin wire around a plastic card were effective at producing a signal. However, the signal amplitude showed a significant asymmetry when the coils were rotated  $180^\circ$  around the vertical  $y$ -axis. The PCB-based coil minimizes this asymmetry.

#### B. Measurement theory

According to Faraday's law, the voltage induced in the pickup coil by the magnetic near-field  $\vec{B} = \vec{B}(x, y)e^{i\omega t}$  is given by

$$V_{coil} = -d/dt(\vec{A} \cdot \vec{B}) = -i\omega A B_x, \quad (3)$$

where  $\vec{A} = A\hat{x}$  gives the effective area of the pickup coil. In order to relate current density  $J(x)$  to the induced pickup coil

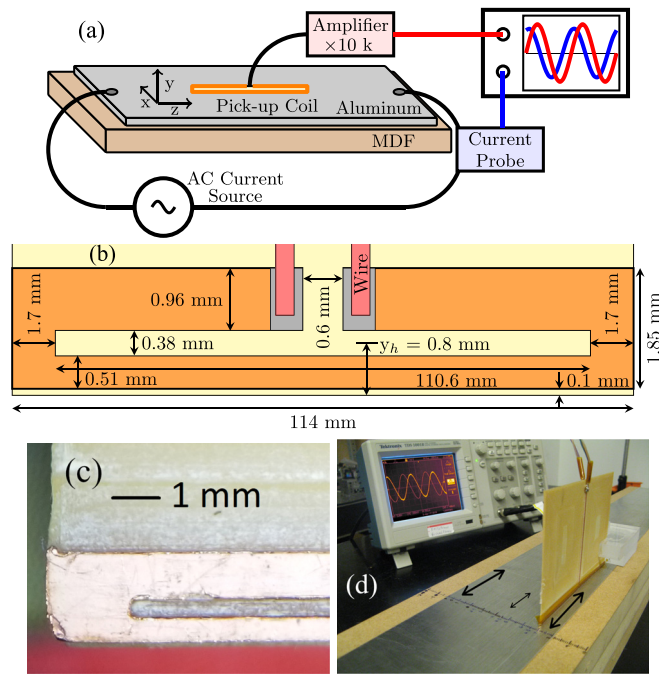


Fig. 3. Experimental system. (a) Experimental setup showing the aluminum strip, ac source, Hall effect current sensor, and pickup coil, which is scanned in the  $x$ -direction. Changes in amplitude and phase between the amplified  $V_{sig}$  and the total current can be seen by plotting both on an oscilloscope. (b) Schematic of the pickup coil. All dimensions have a nominal error of 0.05 mm. (c) The end portion of the pickup coil, showing the milled center channel and length scale. (d) A photograph of the table-top setup, with color adjustment on the oscilloscope screen for clarity. Arrows (black) indicate the current direction and magnitude. The pickup coil PCB is shown with two twisted-pair signal wires attached at the top: final measurements were conducted with only one twisted-pair, which was connected directly onto the pickup coil loop for better fidelity and lower noise.

voltage  $V_{coil}$ , we note that  $\vec{B}(x, y)$  is given by the Biot–Savart integral in the quasi-static limit,

$$\vec{B}(x, y) = \mu_0/2\pi \int \frac{J(x')(-y\hat{x} + (x-x')\hat{y})}{(x-x')^2 + y^2} dx'. \quad (4)$$

However, in the limit that the pickup coil is at the surface of the aluminum strip (i.e.,  $y \rightarrow 0$ ), then  $\vec{B}(x) \simeq \mu_0 J(x)\hat{x}/2$  from Ampère’s law for  $|y| \ll \delta$ . Figure 5 shows that the current distribution  $J(x)$  and the horizontal component  $B_x(x)$ , less than a millimeter from the surface, are proportional to each other (by  $\mu_0/2$ ) near the center of the conductor but deviate from each other at the edges, as shown in Fig. 4.

Therefore, across the middle of the conductor, we have a good approximation,

$$V_{coil}(x) = -i\omega AB_x(x) \simeq -i\omega A \frac{\mu_0}{2} J(x). \quad (5)$$

Since we measure an amplified signal  $V_{sig} \approx V_{coil} \times 10^4$ , calibrations relating  $V_{sig}$  to  $B_x$  and  $J$  are required.

### C. Calibration

We used a two-part calibration procedure. First, the frequency-dependent gain of the coil-amplifier system was examined using the pickup coil to measure the magnetic field near an aluminum rod of the circular cross section. For a known current in the rod, the drop in the signal at higher frequencies can be attributed to the bandwidth of the coil-amplifier system, independent of the skin effect in the rod. Second, we measure the field above the rectangular strip at a low frequency (250 Hz), where the current is nearly evenly distributed. Averaging over the middle region of a known current density allows us to relate the amplified voltage  $V_{sig}$  to the known average current density and the surface magnetic field strength. Measurements of  $V_{sig}$  are divided by the linear  $\omega$  scaling, corrected for frequency dependent amplifier

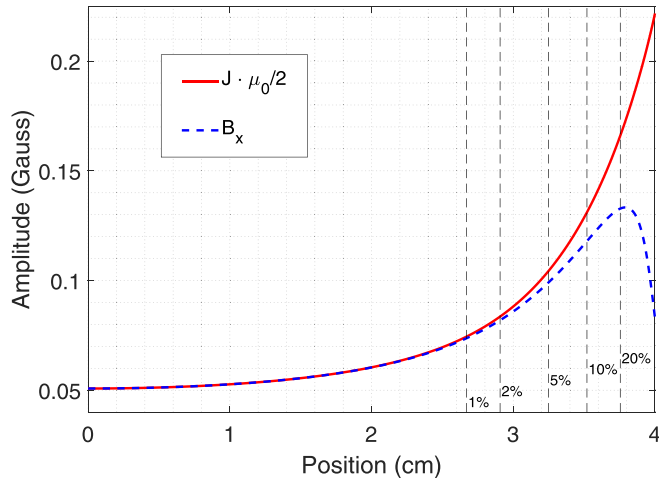


Fig. 4. Plot of the magnetic near field  $B_x$  (dashed blue) and current density  $J$  (solid red) multiplied by  $\mu_0/2$  to demonstrate the close relationship between the two quantities. Values are for 1 A magnitude at 5 kHz, where  $B_x$  is taken at  $y_h = 0.8$  mm. Dashed vertical lines indicate the relative magnitude difference between the two values. We see excellent agreement in the central region, with less than 1% deviation. The difference grows towards the edges, where it exceeds 20%. The relative phases of  $J$  and  $B_x$  (not shown) have similar agreement, within  $\approx 1^\circ$  across the center and diverging to about  $15^\circ$  at the edges.

gain, and multiplied by the voltage-to- $J$  and voltage-to- $B$  factors to produce real values of  $J$  and  $B_x$  for the data in Figs. 5 and 6. The full calibration procedure is detailed in Appendix C.

Phases are measured using the time delay between the zero crossings of the Hall current sensor and  $V_{sig}$ . The phase is presented relative to the  $x=0$  center phase ( $\equiv 0^\circ$ ), since pickup ( $-90^\circ$ ), inversion ( $180^\circ$ ), and bandwidth (unique to frequency) were not studied with sufficient precision.

## IV. RESULTS

The main results of this paper are shown in Figs. 5 and 7, where we plot the amplitude and phase, respectively, of the pickup coil signal vs transverse position  $x$ . The amplitude measurements in Fig. 5 clearly show the ac skin effect: at high frequency (5 kHz), the current is the highest at the edges of the conducting strip, while at a much lower frequency (250 Hz), the current density is essentially uniform. We use two vertical axes in Fig. 5 to show the surface magnetic field  $B_x(x)$  (left) and the current density  $J(x)$  (right) that we convert from the pickup coil signal based on our calibration procedure (see Sec. III B and Appendix C). We have also plotted the theoretical expectations for the current density (solid) and surface magnetic field (dashed) and find good agreement with the data in the center portion of the strip. For completeness, we also present all of our measured data in Fig. 6. At the edges of the strip, the data is lower than the theoretical expectation, possibly due to high field curvature or misalignment of the coil in a region with a significant  $B_y$  component.

The amplitude of the current density and associated surface magnetic field follow a roughly exponential fall off (with an offset) from the edges towards the middle of the strip. We define the characteristic decay constant  $\lambda$  as the distance from the maximum magnitude position to the position where the magnitude falls to  $1/e$  above the minimum value at the center. Table I shows  $\lambda$  for the data at all the

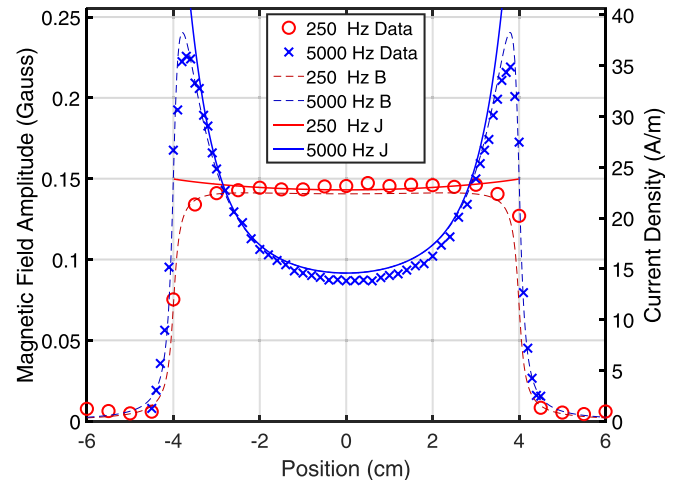


Fig. 5. Pickup coil measurements vs transverse position at 250 Hz (red circles) and 5 kHz (blue crosses) for 1.3 A rms of current. The pickup coil measurements are given in terms of the calibrated surface magnetic field  $B_x$  (left axis) and calibrated current density  $J$  (right axis). The theoretical current density predictions (solid lines) and the surface magnetic field  $B_x$  predictions (dashed lines) at a detector of height  $y_h = 0.8$  mm are shown for the Silvester numerical method (Ref. 15) without any free parameters, using our conductor with a width of 80.1 mm, a height of 0.63 mm, and conductivity  $\sigma = 2.50 \times 10^7 (\Omega\text{m})^{-1}$ . Theoretical current density values reach 62.3 A/m at the edge. Error bars are smaller than the symbol size and are omitted.

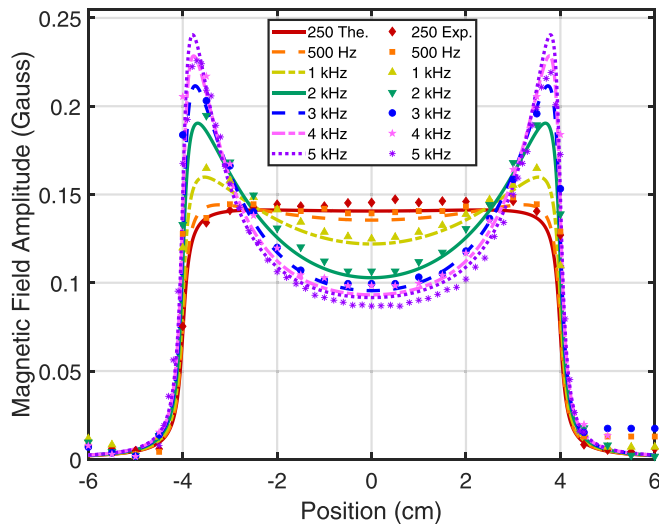


Fig. 6. Comparison of data and theory for all measured frequencies, 250 Hz through 5 kHz. Theory curves use the same parameters as Fig. 5.

frequencies shown in Fig. 6. The theoretical values for the current density and surface magnetic field,  $\lambda_J$  and  $\lambda_{B_{th}}$ , are extracted from numerical simulations (Silvester method<sup>15</sup> for Table I). For interpolation of the data, both a fourth order polynomial and an exponential function yield the same  $1/e$  values for  $\lambda_{B_{exp}}$ . We note that the fall off constant  $\lambda$  is significantly larger than the skin depth  $\delta$ , as expected for the lateral skin effect regime. For example, across the few kHz region of our data, we find that  $\lambda \sim 5\delta$ . Generally,  $\lambda$  depends on the geometry of the strip, which we parameterize by  $WT/\delta^2$ .<sup>26</sup>

In Fig. 7, we plot the phase of the pickup coil signal (relative to the  $x=0$  phase) vs position  $x$  across the strip for a 5 kHz current. The data clearly show that the phase of the current density varies by more than  $30^\circ$  across the strip, in tandem with the magnitude. In other words, for short portions of the ac cycle, the current in the center goes in the opposite direction to the current on the edges of the strip. The theory curve for the phase agrees reasonably well with the data over the breadth of the strip. Past the strip edges, the overall pickup coil signal is weaker, and the data deviate from theory, possibly due to interference in the pickup coil from other parts of the apparatus. Furthermore, in contrast with the magnitude, the phase across the conductor, when plotted, displays a modest “bump” at the center of the strip. This non-monotonic behavior means that for brief moments

Table I. Comparison of the decay constant  $\lambda$ , i.e., the lateral skin “width,” for theory and experiment in units of the skin depth  $\delta$  for data in Fig. 6. The theoretical values for the current density and surface magnetic field (at the probe) are given by  $\lambda_J$  and  $\lambda_{B_{th}}$ , respectively. The experimental value for the surface magnetic field is given by  $\lambda_{B_{exp}}$ , with one standard deviation given in parentheses.

Freq (Hz)	$\delta$ (mm)	$WT/\delta^2$	$\lambda_J/\delta$	$\lambda_{B_{th}}/\delta$	$\lambda_{B_{exp}}/\delta$
250	6.37	0.31	2.3	1.8	(No fit)
500	4.50	0.62	3.2	3.3	2.9 (1.3)
1000	3.18	1.25	4.4	4.8	4.8 (0.3)
2000	2.25	2.49	5.2	6.0	5.6 (0.5)
3000	1.84	3.74	5.1	6.3	5.5 (0.9)
4000	1.59	4.98	4.8	6.3	5.8 (1.0)
5000	1.42	6.23	4.6	6.3	7.0 (1.1)

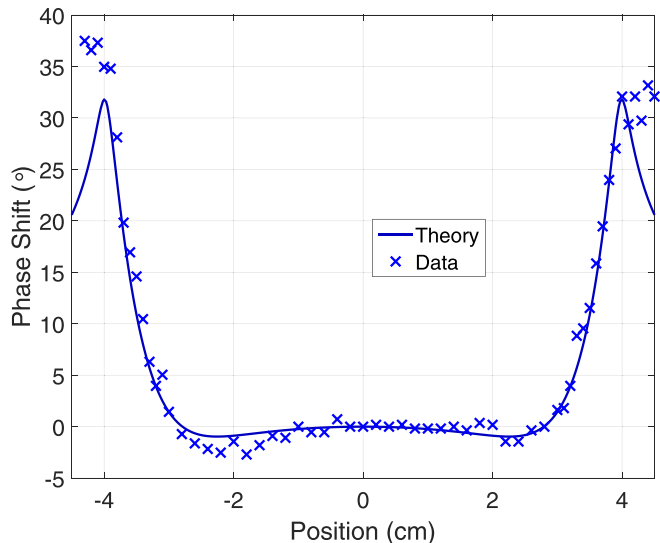


Fig. 7. Pickup coil phase measurements vs transverse position at 5 kHz. The pickup coil measurements (crosses) are compared to the theoretical prediction (line) of the phase of the surface magnetic field  $B_x$  (at a height  $y_h = 0.8$  mm) based on the same numerical calculation employed for the theory curves in Fig. 5. The phases are given relative to the center value at  $x=0$ . Errors are smaller than the symbol size and are omitted.

in the cycle, the current at the center and along the edges of the strip goes in the same direction, but the current between these regions goes in the opposite direction. This counterflow behavior is examined in detail in Appendix B.

## V. CONCLUSION

We have directly observed the ac skin effect at kHz frequencies in a rectangular aluminum strip. We have shown experimentally that the current increasingly hugs the edges of the strip as the frequency increases and that the phase of the current density varies significantly across the strip. We have calculated the theoretical distribution of the current across the strip by four different methods and find good agreement between these and the data, with modest deviations at the edge.

Conveniently, our simple experimental setup is well suited to an in-class demonstration. The setup requires standard laboratory equipment (analog controlled current source, function generator, op-amp-based amplifier, current sensor, and oscilloscope) and a lab-built elongated pickup coil. A possible upgrade to the pickup coil is to use two perpendicular elongated coils so that  $B_x$  and  $B_y$  can be measured simultaneously. Such a pickup coil would provide more information when probing the edges of the strip and the circular polarization in the case of phased currents in multiple strips.

This kHz-level work is a stepping stone towards accurate engineering of GHz-level microwave magnetic near-fields with much smaller conducting strips ( $\sim 100 \mu\text{m}$ ) on an atom chip. Based on the principle of similitude, the agreement between theory and experiment in this kHz work provides confidence that our numerical computation methods for the ac skin effect and related magnetic near field can be extended to microwave frequencies.

## ACKNOWLEDGMENTS

This work was supported in part by AFOSR, NSF, DTRA, and William & Mary.

## APPENDIX A: ANALYTIC FORMS

In the interest of supplying useful analytic functions to the experimenters with similar flat wires, here we reproduce two functions from the paper by Belevitch *et al.*<sup>27</sup> for the case of a flat, 1D “ribbon” conductor of width  $2W$  and thickness  $2T$ , where  $W \gg T$ . Solutions assume the form of an infinite sum of even powers of the normalized  $x$  coordinate  $s = x/W$ ,

$$J(s) = \sum_{n=0}^N C_n \cdot s^{2n}, \quad (\text{A1})$$

where increasing the order  $N$  of the sum yields higher accuracy. To simplify some expressions, Belevitch *et al.*<sup>27</sup> used the dimensionless variable  $k = i\omega\sigma\mu WT/\pi = i(2WT/\pi\delta^2)$  and dc linear current density  $J_{dc} = I_{ext}/2W$ . In our experiment,  $|k| \approx 0.2$  at 250 Hz and  $|k| \approx 4$  at 5 kHz. This method’s first-order ( $N = 1$ ) solution yields a complex quadratic equation,

$$J(s) = \frac{1 + k + ks^2}{1 + \frac{4}{3}k} \cdot J_{dc},$$

which applies only for sufficiently low frequencies (i.e.,  $|k| < 0.1$ ). For larger  $|k|$ , more terms in Eq. (A1) must be included.

In Fig. 8, we plot  $C_n$  terms in the sum of Eq. (A1) for different values of  $|k|$  with  $N = 500$ . Each segmented line connects consecutive  $C_n$  terms in sequence, beginning in the lower right with the  $C_0$  or dc value and ending for converged sequences with many values near the origin, contributing very little. Solutions require many powers of  $s$  for convergence at high frequency, while only a few are needed for low frequency convergence. At low frequencies (e.g.,  $|k| = 0.02$ ), similar to the discussion in Sec. II A, the primary contribution is largely real, with a small imaginary  $s^2$  contribution. The leading  $C_0$  terms describe a semi-circle of diameter  $\approx 0.36 \approx 1 - 2/\pi$ , a feature also described in Casimir and Ubbink’s analysis.<sup>8</sup>

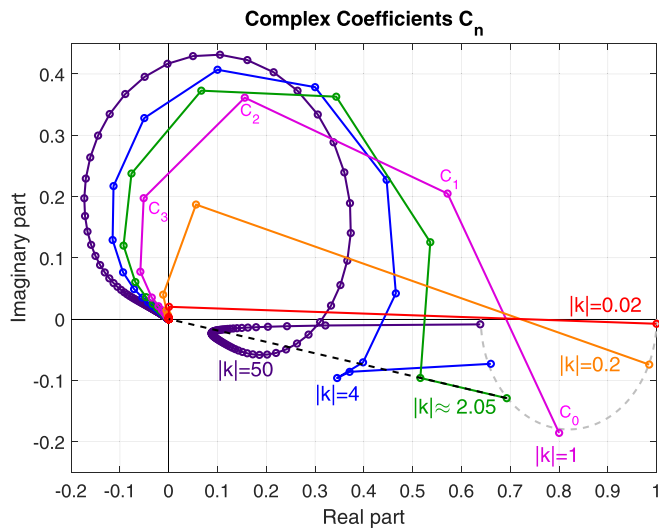


Fig. 8. Sequential complex values of the coefficients  $C_n$  for  $N = 500$ . Each colored line connects consecutive terms for a single frequency, labeled by  $|k|$ . Selectively shown are the lowest and highest experimental frequencies used ( $|k| = 0.2$  and 4) and  $|k| \approx 2.05$ , the value at which the “counterflow” effect begins.

In the high frequency limit of a thin ribbon conductor, e.g.,  $|k| \gg 50$ , Belevitch also provided an exact solution for the magnitude of the current distribution,

$$|J(s)| = \frac{2}{\pi\sqrt{1-s^2}} \cdot J_{dc}. \quad (\text{A2})$$

This function appears, scaled to our parameters, in Fig. 1. This expression also shows that in the center of a very thin strip, the minimum  $J$  will only drop to  $2/\pi \approx 0.63662$  times the dc value. Our other simulations reinforce the trend toward this curve at higher frequencies. The phase in the high frequency limit approaches a uniform distribution, lagging the driving current by  $90^\circ$  (for a very thin ribbon).

## APPENDIX B: THE COUNTERFLOW EFFECT

Due to the phase-shifting of the skin effect, the dominant outer current always precedes the rest of the current (see Fig. 9). However, above some frequency, the phase in the center slightly precedes the area surrounding it. As seen in Fig. 7, a slight bump in phase is present at the center of the strip.

As shown in Fig. 9 (3, 4, and 5 kHz curves), for a small portion of time (about  $1^\circ$ , twice per cycle), the currents in the center and edge go in the same direction, but currents at points between flow in the opposite direction, near the zero crossing of a current oscillation. Our calculations show that this effect begins at  $|k| \approx 2.0514$ , which corresponds to about 2.6 kHz in our experiment. The effect grows and then diminishes at very high frequencies, and we predict no higher order phase reversals.

We find that we are able predict this crossing point analytically, using the Belevitch model. Using  $s = x/W$ , the current at any point can be represented by the expression

$$J(s) = a(s) + ib(s) = \sum_{n=0}^N (a_n + ib_n)s^{2n},$$

with phase  $\phi$  given by

$$\phi = \tan^{-1} \left[ \frac{b(s)}{a(s)} \right].$$

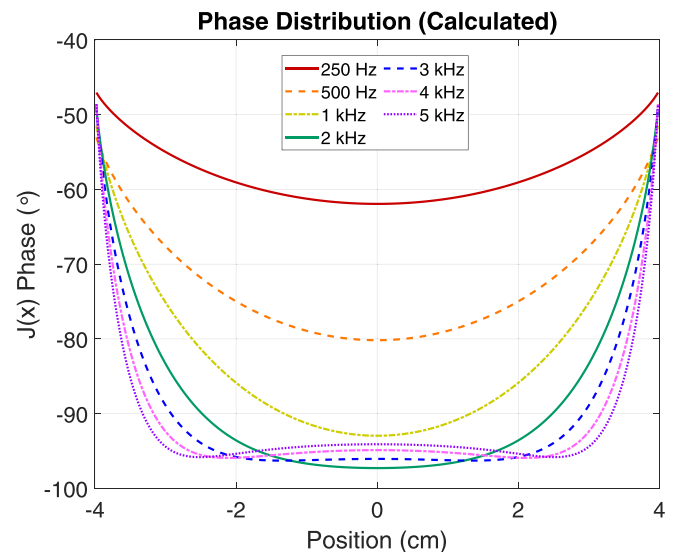


Fig. 9. Phase distributions calculated using the Silvester model (Ref. 15) for the experimental parameters given in Fig. 5. Note that the counterflow effect is visible for 3 kHz and higher.

The phase bump appears when the curvature of  $\phi$  at  $s=0$  flips from negative to positive. Setting  $d^2\phi/ds^2 = 0$ , we obtain at  $s=0$  (a prime represents a derivative with respect to  $s$ )

$$\frac{a''}{a} = \frac{b''}{b},$$

where we have used the fact that  $d\phi/ds = 0$  at  $s=0$  due to the even symmetry of  $J(s)$ . We can translate the above conditions into statements about relative curvature of the real and imaginary parts of the current density at the center,

- If  $a''/a > b''/b$ , the center phase always follows locally.
- If  $a''/a = b''/b$ , the center is in phase with its surroundings.
- If  $a''/a < b''/b$ , the center phase precedes locally.

Using the summation  $J(s) = C_0 + C_1s^2 + C_4s^4 + \dots$ , we can identify  $C_0 = a + ib|_{s=0}$  and  $C_1 = 1/2!(a'' + ib'')|_{s=0}$ . We only need to compute two complex terms of Eq. (A1)'s solution,  $C_0$  and  $C_1$ , to know whether the current has this phase reversal at the center. The equality condition  $a''/a = b''/b$  implies that  $C_0$  and  $C_1$  lie on a line through the origin (see the dashed line in Fig. 8). Numerically, we find that this happens for  $|k| = 2.0514 \approx 2$ . The frequency required for this central phase reversal effect is then roughly  $f_\phi \approx 1/WT \mu \sigma$ . At higher frequencies, the effect is at most only a few degrees, which is sufficient for observation (see Fig. 7).

## APPENDIX C: CALIBRATION

In principle, we can extract values of  $J(x)$  or  $B(x)$  via Eq. (5), a measurement of  $V_{coil}(x)$ , the frequency  $\omega$ , and the coil area  $A$ , but this approach is problematic. First, the coil area is not well defined because the coil's enclosed area is comparable to the wire area (see Figs. 3(b) and 3(c)). Second, the signal we measure on the oscilloscope  $V_{sig}$  is also modified by the bandwidth of the amplifier. Finally,  $V_{coil}$  may have additional magnetic gradient dependence or  $\omega$ -dependence beyond the linear  $\omega$  scaling in Eq. (3).

We resolve these difficulties by using a collective model for the gain of the pickup coil system (coil, amplifier, etc.) that relates  $V_{sig}$  to the current density and magnetic field at the surface,

$$J(x) = \frac{\alpha_J(\omega)V_{sig}(x)}{\omega}, \quad \text{and} \quad B_{surf}(x) = \frac{\alpha_B(\omega)V_{sig}(x)}{\omega}.$$

The proportionality constants  $\alpha_J(\omega)$  and  $\alpha_B(\omega)$  are determined via calibration experiments at known  $J$  and  $B_{surf}$ . These two constants also have the same frequency dependence, so for two different frequencies  $\omega$  and  $\omega_0$ , we expect  $\alpha_J(\omega)/\alpha_J(\omega_0) = \alpha_B(\omega)/\alpha_B(\omega_0)$ . From this relation, we see that we have  $\alpha_J(\omega) = \alpha_J(\omega_0)(\alpha_B(\omega)/\alpha_B(\omega_0))$ , so we can obtain  $\alpha_J(\omega)$  from measurements of  $\alpha_J(\omega_0)$  and  $\alpha_B(\omega)/\alpha_B(\omega_0)$ .

We measure  $\alpha_J(\omega_0)$  at a very low frequency with  $\omega_0 = 2\pi \times 250$  Hz, where the ac skin effect is near negligible yet high enough in frequency to be visibly picked up by the coil. The current density  $J(x)$  is near-constant across the middle of the strip as seen in Fig. 5.

We determine  $\alpha_B(\omega)/\alpha_B(\omega_0)$ , i.e., the frequency dependent gain of the pickup coil system, by measuring  $V_{sig}$  at the surface of an aluminum rod of the circular cross section driven by a

known ac for different frequencies. Due to its geometry, the external magnetic field of the rod is frequency independent (unlike the strip), so we can use  $\alpha_B(\omega)/\alpha_B(\omega_0) = (V_{sig}(\omega_0)/\omega_0)/(V_{sig}(\omega)/\omega)$  to determine the  $\alpha_B(\omega)/\alpha_B(\omega_0)$  calibration ratio.

<sup>a)</sup>Electronic mail: saaubi@wm.edu

<sup>1</sup>T. J. Higgins, "The origins and developments of the concepts of inductance, skin effect and proximity effect," *Am. J. Phys.* **9**, 337–346 (1941).

<sup>2</sup>J. C. Maxwell, *A Treatise on Electricity and Magnetism* (Oxford U. P., Oxford, 1873), Vol. 2.

<sup>3</sup>J. J. Thomson, *Notes on Recent Researches in Electricity and Magnetism: Intended as a Sequel to Professor Clerk-Maxwell's Treatise on Electricity and Magnetism* (Clarendon Press, Oxford, 1893).

<sup>4</sup>Oliver Heaviside, *Electromagnetic Theory* (Electrician Print and Publishing Company, 1893), Vol. 1.

<sup>5</sup>J. W. Strutt, "On the self-induction and resistance of straight conductors," *Philos. Mag.* **21**, 381–394 (1886).

<sup>6</sup>W. Thomson, *Mathematical and Physical Papers: Elasticity, Heat, Electro-Magnetism* (Clarendon Press, London, 1890), Vol. 3.

<sup>7</sup>E. Rutherford, "Magnetization of iron by high-frequency discharges," *Trans. N. Z. Inst.* **27**, 481–513 (1894), available at <http://rsnz.natlib.govt.nz/>.

<sup>8</sup>H. B. G. Casimir and J. Ubbink, "The skin effect introduction; the current distribution for various configurations," *Philips Tech. Rev.* **28**, 271–283 (1967), available at [https://www.pearl-hifi.com/06\\_Lit\\_Archive/02\\_PEARL\\_Arch/Vol\\_16/Sec\\_53/Philips\\_Tech\\_Review/](https://www.pearl-hifi.com/06_Lit_Archive/02_PEARL_Arch/Vol_16/Sec_53/Philips_Tech_Review/).

<sup>9</sup>H. B. G. Casimir and J. Ubbink, "The skin effect at high frequencies," *Philips Tech. Rev.* **28**, 300–315 (1967), available at [https://www.pearl-hifi.com/06\\_Lit\\_Archive/02\\_PEARL\\_Arch/Vol\\_16/Sec\\_53/Philips\\_Tech\\_Review/](https://www.pearl-hifi.com/06_Lit_Archive/02_PEARL_Arch/Vol_16/Sec_53/Philips_Tech_Review/).

<sup>10</sup>H. B. G. Casimir and J. Ubbink, "The skin effect in superconductors," *Philips Tech. Rev.* **28**, 366–386 (1967), available at [https://www.pearl-hifi.com/06\\_Lit\\_Archive/02\\_PEARL\\_Arch/Vol\\_16/Sec\\_53/Philips\\_Tech\\_Review/](https://www.pearl-hifi.com/06_Lit_Archive/02_PEARL_Arch/Vol_16/Sec_53/Philips_Tech_Review/).

<sup>11</sup>P. Silvester, "The accurate calculation of skin effect in conductors of complicated shape," *IEEE Trans. Power Appar. Syst.* **87**, 735–742 (1968).

<sup>12</sup>P. Silvester, "Modal network in flat theory of skin effect conductors," *Proc. IEEE* **54**, 1147–1151 (1966).

<sup>13</sup>P. Silvester, "Ac resistance and reactance of isolated rectangular conductors," *IEEE Trans. Power Appar. Syst.* **86**, 770–774 (1967).

<sup>14</sup>P. Silvester, "Network analog solution of skin and proximity effect problems," *IEEE Trans. Power Appar. Syst.* **86**, 241–247 (1967).

<sup>15</sup>P. Silvester, *Modern Electromagnetic Fields* (Prentice Hall, Englewood Cliffs, NJ, 1968).

<sup>16</sup>G. Antonini, A. Orlandi, and C. R. Paul, "Internal impedance of conductors of rectangular cross section," *IEEE Trans. Microwave Theory Tech.* **47**, 979–985 (1999).

<sup>17</sup>T. Vu Dinh, B. Cabon, and J. Chilo, "New skin-effect equivalent circuit," *Electron. Lett.* **26**, 1582–1584 (1990).

<sup>18</sup>S. Mei and Y. I. Ismail, "Modeling skin and proximity effects with reduced realizable RL circuits," *IEEE Trans. VLSI Syst.* **12**, 437–447 (2004).

<sup>19</sup>R. Faraji-Dana and Y. Chow, "Edge condition of the field and ac resistance of a rectangular strip conductor," *IEE Proc. H* **137**, 133–140 (1990).

<sup>20</sup>D. Kajfez, J. Guo, and A. W. Glisson, "Magnetic field patterns inside strip conductors," *Microwave Opt. Technol. Lett.* **20**, 272–274 (1999).

<sup>21</sup>J. Guo, D. Kajfez, and A. W. Glisson, "Skin-effect resistance of rectangular strips," *Electron. Lett.* **33**, 966–967 (1997).

<sup>22</sup>M. Vitelli, "Calculation of per-unit-length resistance and internal inductance in 2-d skin-effect current driven problems," *IEEE Trans. Electromagn. Compat.* **44**, 529–538 (2002).

<sup>23</sup>M. Matsuki and A. Matsushima, "Efficient impedance computation for multiconductor transmission lines of rectangular cross section," *Prog. Electromagn. Res.* **23**, 373–391 (2012).

<sup>24</sup>R. Faraji-Dana and Y. L. Chow, "The current distribution and ac resistance of a microstrip structure," *IEEE Trans. Microwave Theory Techn.* **38**, 1268–1277 (1990).

<sup>25</sup>V. Belevitch, "The lateral magnetic skin-effect in thin plates," *Philips Res. Rep.* **31**, 199–215 (1976), available at [https://www.pearl-hifi.com/06\\_Lit\\_Archive/02\\_PEARL\\_Arch/Vol\\_16/Sec\\_53/Philips\\_Rsrch\\_Reports\\_1946\\_thru\\_1977/](https://www.pearl-hifi.com/06_Lit_Archive/02_PEARL_Arch/Vol_16/Sec_53/Philips_Rsrch_Reports_1946_thru_1977/).

<sup>26</sup>V. Belevitch, "The lateral skin effect in a flat conductor," *Philips Tech. Rev.* **32**, 221–231 (1971), available at [https://www.pearl-hifi.com/06\\_Lit\\_Archive/02\\_PEARL\\_Arch/Vol\\_16/Sec\\_53/Philips\\_Tech\\_Review/](https://www.pearl-hifi.com/06_Lit_Archive/02_PEARL_Arch/Vol_16/Sec_53/Philips_Tech_Review/).

<sup>27</sup>V. Belevitch, P. Gueret, and J. C. Lienard, "Le skin-effet dans un ruban," *Rev. HF* **5**, 109–115 (1962).

- <sup>28</sup>G. S. Smith, "On the skin effect approximation," *Am. J. Phys.* **58**, 996–1002 (1990).
- <sup>29</sup>G. S. Smith, "A simple derivation for the skin effect in a round wire," *Eur. J. Phys.* **35**, 025002 (2014).
- <sup>30</sup>N. Gauthier, "Explaining the skin effect simply, with  $V = RI + L (di/dt)$ ," *Am. J. Phys.* **54**, 649–650 (1986).
- <sup>31</sup>D. Gerling, "Approximate analytical calculation of the skin effect in rectangular wires," in *International Conference on Electrical Machines and Systems ICEMS 2009* (IEEE, 2009), pp. 1–6.
- <sup>32</sup>Z. Popovic and B. Popovic, *Introductory Electromagnetics* (Prentice Hall, 2000), Chap. 20, pp. 382–392.
- <sup>33</sup>This calculation was done using formulas from the paper of Smith.<sup>29</sup> The formulas are the following (they are approximations for the high frequency limit, i.e., wire radius  $\gg$  skin depth):  $R_{ac}/R_{dc} = (1/2)(r/\delta)$ ,  $(L_{ac}/L_{dc}) = 1/(0.5 * (r/\delta))$ , with  $\delta = \sqrt{2/\sigma\mu\omega}$ .
- <sup>34</sup>J. R. Gosselin, P. Rochon, and N. Gauthier, "Study of eddy currents in a cylindrical wire: An undergraduate laboratory experiment," *Am. J. Phys.* **50**, 440–443 (1982).
- <sup>35</sup>J. W. MacDougall, "An experiment on skin effect," *Am. J. Phys.* **44**, 978–980 (1976).
- <sup>36</sup>C. T. Fancher, A. J. Pyle, A. P. Rotunno, and S. Aubin, "Microwave ac Zeeman force for ultracold atoms," *Phys. Rev. A* **97**, 043430 (2018).
- <sup>37</sup>M. K. Ivory, A. R. Ziltz, C. T. Fancher, A. J. Pyle, A. Sensharma, B. Chase, J. P. Field, A. Garcia, D. Jervis, and S. Aubin, "Atom chip apparatus for experiments with ultracold rubidium and potassium gases," *Rev. Sci. Instrum.* **85**, 043102 (2014).
- <sup>38</sup>P. Böhi, M. F. Riedel, T. W. Hänsch, and P. Treutlein, "Imaging of microwave fields using ultracold atoms," *Appl. Phys. Lett.* **97**, 051101 (2010).
- <sup>39</sup>H. Tsuboi and K. Kunisue, "Eddy current analysis of thin plates taking account of the source current distributions and its experimental verifications," *IEEE Trans. Magn.* **27**, 4020–4023 (1991).
- <sup>40</sup>We learned of this work after submission of the manuscript.
- <sup>41</sup>T. H. Petersen, K. H. Carpenter, and C. M. May, "Comparison of experimental measurements of current distribution in a flat conductor with simulated results from the partial inductance method," *IEEE Trans. Electromagn. Compat.* **51**, 345–350 (2009).
- <sup>42</sup>M. Kosek, M. Truhlar, and A. Richter, "Skin effect in massive conductors at technical frequencies," *Przeł. Elektrotech.* **5**, 179–185 (2011), available at <http://pe.org.pl/index.php?lang=1>.
- <sup>43</sup>M. Kosek, M. Truhlar, and A. Richter, "Skin effect in conductor of rectangular cross-section—approximate solution," *Przeł. Elektrotech.* **88**, 23–25 (2012), available at <http://pe.org.pl/index.php?lang=1>.
- <sup>44</sup>I. Manke, N. Kardjilov, M. Strobl, A. Hilger, and J. Banhart, "Investigation of the skin effect in the bulk of electrical conductors with spin-polarized neutron radiography," *J. Appl. Phys.* **104**, 076109 (2008).
- <sup>45</sup>A. J. Illott, S. Chandrashekar, A. Kloeckner, H. J. Chang, N. M. Trease, C. P. Grey, L. Greengard, and A. Jerschow, "Visualizing skin effects in conductors with MRI: 7Li MRI experiments and calculations," *J. Magn. Resonance* **245**, 143–149 (2014).
- <sup>46</sup>J. Wagner and M. Syed, "Investigation of skin effect in mercury using a simple solenoid setup," *Am. J. Phys.* **79**, 850–855 (2011).
- <sup>47</sup>H. B. Dwight, "Skin effect in tubular and flat conductors," *Trans. Am. Inst. Electr. Eng.* **37**, 1379–1403 (1918).
- <sup>48</sup>D. R. Lide, *CRC Handbook of Chemistry and Physics* (CRC Press, 1998), Vol. 79.
- <sup>49</sup>The infinite half-space conductor can also be solved analytically.<sup>32</sup>
- <sup>50</sup>See supplementary material at <http://dx.doi.org/10.1119/10.0001272> for an animation which illustrates the time-evolving nature of the current density's phase and amplitude across a wide range of frequencies.
- <sup>51</sup>A. Zangwill, *Modern Electrodynamics* (Cambridge U. P., 2013).
- <sup>52</sup>Both FEKO and Flux are distributed by Altair Inc.
- <sup>53</sup>Older versions of FEKO (before 2019) appeared to use a pseudo-random arrangement of mesh elements, which led to overall continuous and comparable results. Newer versions use regions of aligned rows of uniform triangle mesh elements, and we observe deviations, such as those evident in the amplitude and phase at the center of the strip in Fig. 1, occurring at the borders between these uniform regions.

### ALL BACK ISSUES ARE AVAILABLE ONLINE

The contents of the *American Journal of Physics* are available online. AJP subscribers can search and view full text of AJP issues from the first issue published in 1933 to the present. Browsing abstracts and tables of contents of online issues and the searching of titles, abstracts, etc. is unrestricted. For access to the online version of AJP, please visit <http://aapt.org/ajp>.

Institutional and library ("nonmember") subscribers have access via IP addresses to the full text of articles that are online; to activate access, these subscribers should contact AIP, Circulation & Fulfillment Division, 800–344–6902; outside North American 516–576–2270 or [subs@aip.org](mailto:subs@aip.org).

APPT (individual) members also have access to the American Journal of Physics Online. Not a member yet? Join today <http://www.aapt.org/membership/joining.cfm>. Sign up for your free Table of Contents Alerts at [http://www.aip.aapt.org/features/toc\\_email\\_alerts](http://www.aip.aapt.org/features/toc_email_alerts).